



MOTION PREDICTIONS OF SHIPS IN ACTUAL OPERATING CONDITIONS USING POTENTIAL FLOW BASED SOLVER

M. M. Rahaman¹, H. Islam², H. Akimoto³ and M. R. Islam¹

¹Department of Naval Architecture and Marine Engineering, Bangladesh University of Engineering and Technology, Dhaka-1000, Bangladesh, mashiurrahaman@name.buet.ac.bd; rafiqis@gmail.com

²CENTEC, Instituto Superior Tecnico, University of Lisbon, Portugal, hafiz2612@gmail.com

³Center for the Advancement of Research and Education Exchange Network in Asia (CAREN), Graduate School of Engineering, Osaka University, 2-1 Yamadaoka, Suita, Osaka, Japan 565-0871, akimoto@naoe.eng.osaka-u.ac.jp

Abstract:

Prediction of ship's response in real voyage condition is essential for efficient ship design. At sea, ships rarely voyage in head wave conditions, and mostly prefer oblique waves for lower resistance and better propulsion. This paper provides oblique wave simulation results for a container, tanker and bulk carrier using a commercial potential flow (PF) based solver, HydroSTAR. Although, PF codes have limitation regarding resistance prediction, they are well reliable in predicting ship motion in waves. The paper aims at providing a relative comparison in trends of ship resistance and motion at different heading angles, for three popular ship models, KCS, KVLCC2 and JBC. The paper should prove useful to both ship builders and sailors for optimal design and weather routing.

Keywords: Actual voyage condition; potential flow; added resistance and motion, oblique waves, KCS, KVLCC2, JBC.

1. Introduction

Present day challenge in shipping and shipbuilding industry is the minimization of energy consumption, assurance of maximum protection for marine environment and maximization of efficiency and economy of maritime operations along with safety and comfort. Thus, shipbuilders are emphasizing more and more on reliable resistance and motion prediction for ships at design stage. For shipbuilders, head wave condition is most important, since ship's propulsion power is mostly decided based on head wave condition. However, mariners rarely set voyage routes in head waves, since it offers highest resistance. For mariners, resistance in different oblique waves is of higher importance, since it can help them select the optimum route for voyage. This paper provides a case study for relative comparison of resistance and motion at bow, beam, stern and following wave conditions.

Ships mostly follow oblique waves to minimize the resistance and maximize fuel efficiency. However, study on added resistance prediction in oblique waves has been very limited so far. Among the recent works, Chan et al. (2002) introduced a time domain simulation method incorporating non-linear Euler equations of motion, to predict large amplitude of a Ro-Ro ship in regular oblique waves in an intact and damaged condition. He showed good agreement with measured data except in roll-resonant region, where non-linear effects are significant. Later Orihara (2005) conducted Reynolds averaged Navier-Stokes (RaNS) simulation for SR108 container ship for oblique regular and irregular waves and achieved good agreement with experimental data. However, he used a modified hull shape at stern section. Chen et al. (2010), used time domain Rankine panel method to predict motion of a container vessel in oblique waves together with an artificial spring model to control sway and yaw motion and empirical method for roll damping. Whereas, Song et al. (2011) applied the concept of weakly nonlinear formulation to 3D Rankine panel method based on time domain approach to predict nonlinear motions and hull-grinder loads of a container ship in oblique waves. Ming et al. (2013), used RaNS equation and kinematics equations of rigid body to solve a moving grid, together with sliding grid technique to simulate motion of surface combatant with heave, pitch and roll free motion. The results were compared with linear strip theory and showed good agreement. Duan and Li (2013) used a method combining Gerritsma and Beukelman (G & B) together with Salvesen-Tuck-Faltinsen (STF) and DSG method. He used the method to calculate added resistance profile for whole wave length range in oblique waves for a container and a tanker

ship. Chuang and Steen (2013) also used STF strip theory to directly calculate speed loss of a tanker vessel due to oblique waves.

Oblique wave experiments are generally difficult to perform because of the limited width of wave tanks, which doesn't allow sufficient run duration to reach stability. Recently constructed wave tank facilities may provide solution to such limitations, however they are quite expensive. In case of RaNS solvers, generally, in head wave cases, simulation is run assuming symmetry condition (only for starboard or port side of the ship) with just heave and pitch free motion, whereas for oblique waves, full hull is to be simulated for realizing the effects and to account for the rotational motions. Thus, running simulation in oblique waves increases computational cost by almost twice. Although, Potential Flow based methods predict resistance in oblique waves with limited accuracy because of the high non-linearity involved in such simulations, their motion prediction is in usable level. And, even though, the resistance prediction is not reliable, the trend it produces for different heading angles is enough to develop an understanding regarding resistance encountered in oblique waves.

This paper presents resistance and motion prediction for a container carrier, a tanker ship and a bulk carrier using a potential flow based solver named HydroSTAR, in different oblique waves to show how motion and resistance of ship changes with heading angle with respect to incoming wave direction. The paper emphasizes more on the trend of resistance and motion at different heading angles, rather than the predicted values, since simulation accuracy couldn't be validated.

2. Computational Method and Ship Model

2.1 Mathematical model of the solver

The potential flow based solver used here, HydroSTAR, is a commercial solver developed by BUREAU VERITAS, France. The solver has been under development since 1991 and provides a complete solution of first order low-frequency wave loads for floating body with or without forward speed in deep water and in finite water depth. The theoretical detail of the code has been elaborately explained by Chen (2004, 2009) in his papers. A brief overview on the solver is described below following Chen's papers and thesis of Kumar (2014).

HydroSTAR follows an earth fixed and a body fixed Cartesian coordinate systems both of which follow same sign rule, the Z axis is upward positive and X is positive in the direction of flow propagation. The solver follows Laplace equation, $\varphi_{yy}^N + \varphi_{zz}^N = 0$, that is, the radiation potential in y and z direction is zero. The linear free surface boundary condition is given by $-\omega^2 \varphi_j^N + g \frac{\delta}{\delta z} \varphi_j^N = 0$, at $z = 0$. Bottom boundary condition, $\nabla \varphi^N \rightarrow 0$, on $z \rightarrow -\infty$, and radiation condition at infinity, $\frac{\delta \varphi^N}{\delta r} - i \frac{\omega^2}{g} \varphi^N = 0$, $|r| \rightarrow \infty$. The time dependent fluid motion is considered to be simple harmonic and the velocity potential is given by,

$$\Phi = \text{Re} [\varphi(x, y, z) e^{-i\omega t}] \tag{1}$$

$$\varphi = -i\omega [(\varphi_o + \varphi_7)\zeta_{\alpha} + (X_i \varphi_i)] \tag{2}$$

$$\varphi_o = \frac{-ig\zeta_{\alpha} \cosh[k(z+h)]}{\omega \cosh kh} e^{ik(x \cos \alpha - y \sin \alpha)} \tag{3}$$

In above equations, φ is the potential with subscript defining the direction and superscript the type of potential, ω is the frequency of incoming incident waves, g is the gravitational constant. φ_o is the incident wave potential, φ_7 is diffraction wave potential, ζ_{α} is incident wave amplitude and α is wave heading angle.

The integral equation of the first-order problem is derived by making use of the Green function,

$$\varphi_i(x, y, z) = \frac{1}{4\pi} \iint_S \sigma_j(\xi, \eta, \zeta) G(x, y, z; \xi, \eta, \zeta) ds \tag{4}$$

where, (ξ, η, ζ) refers to a point on surface S and $\sigma_j(\xi, \eta, \zeta)$ represents unknown source distribution. The finite-depth Green function is decomposed into the deep-water Green function and two regular functions representing the influence of the seabed. The regular functions are evaluated accurately and approximated by Chebyshev polynomials of three variables.

To construct the solver, in the momentum equation, a fictitious force depending on the fluid velocity is introduced to represent the energy dissipation of various sources without modifying the inviscid and irrotational properties. Thus, a damping term with the same parameter is present in the classical boundary condition over the free surface. By applying the perturbation procedure, the boundary value problems of the first order and second order are then developed.

The first order wave exciting forces and oscillatory forces created by the dynamic pressure acting on the rigid body is obtained by,

$$F_k e^{-i\omega t} = -i\rho\omega e^{-i\omega t} \int [\varphi_{\sigma} + \varphi_{\tau}] n_k ds \quad (5)$$

$$F_{kj} = -\rho\omega^2 e^{-i\omega t} \sum_{j=1}^6 \iint \varphi_j n_k ds \quad (6)$$

Here, F_k represents the k-th component of wave exciting forces and F_{kj} represents the k-th component of force caused by the motion in j-th direction. Here, like j, k also represents degree of freedom of motion. The added mass and damping coefficients are respectively represented by,

$$a_{ki} = -\rho \cdot Re[\iint \varphi_j n_k ds] \quad (7)$$

$$b_{kj} = -\rho\omega \cdot Im[\iint \varphi_j n_k ds] \quad (8)$$

Finally, the equation of motion in frequency domain is represented by,

$$\sum_{j=1}^6 (M_{kj} + a_{ki}) \ddot{X}_j + b_{ki} \dot{X}_j + cX_j = F_k; \quad k = 1,2,3, \dots, 6; j = 1,2,3, \dots, 6 \quad (9)$$

Here, M_{ki} is the inertia matrix in k direction due to j motion, c is hydrostatic restoring force coefficient matrix, X_j is the vector containing three translational and rotational oscillations about the co-ordinate axes in j-direction, and F_k is the wave exciting force in k-direction.

To deal with irregular frequencies, mathematical model has been used. First, location of the irregular frequencies is determined by the Eigen-frequencies and then they are eliminated using extended integral equation method.

2.2 Ship models

Three different ship models have been simulated in oblique waves in this paper. The models are KRISO Container Ship (KCS) in S. (2008), KRISO Very Large Crude Carrier 2 (KVLCC2) in S. (2008) and Japan Bulk Carrier (JBC) in T. (2015).

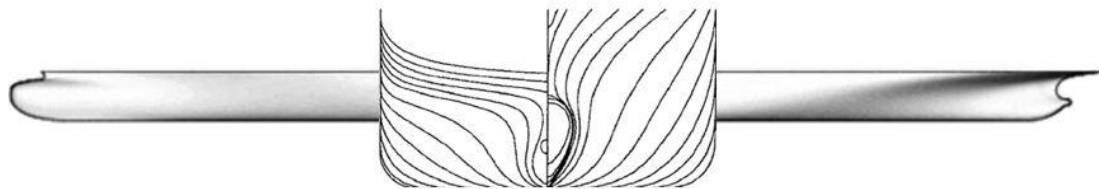


Fig. 1: Body plan of KCS model

The KCS is a 3600TEU capacity container ship model designed by KRISO (formerly MOERI) for research purpose. The ship is a very popular test model, as many experimental and CFD test results are open to public

and have been discussed in many workshops and conferences like Gothenburg, Tokyo and SIMMAN workshops. Figure 1 shows the body plan of KCS model, and the ship specifications are provided in Table 1.

Table 1: Specifications of a KCS model ship

Specification	Scale	KCS ship (full scale)
Length between perpendicular	L _{pp} (m)	230.0
Breadth	B (m)	32.2
Depth	D (m)	19.0
Draft	T (m)	10.8
Wetted surface area	S (m ²)	9530
Displacement volume	V (m ³)	52030
LCB from mid-ship (fwd+)	LCB (%)	-1.48
K _{yy}	K _{yy} (%)	0.25 L _{pp}

KVLCC2 is another model provided by KRISO and is equally popular among researchers as like KCS. Table 2 provides the specifications of the KVLCC2 model and Figure 2 shows its side view and body plan.

Table 2: Specifications of the oil tanker ship model KVLCC2

Specification	Unit	KVLCC2 ship (full scale)
Length between perpendicular	L _{pp} (m)	320.0
Breadth	B (m)	58.0
Depth	D (m)	30.0
Draft	T (m)	20.8
Wetted surface area	S (m ²)	27194.0
Displacement volume	V (m ³)	312622
LCB from mid-ship	LCB (m)	11.136
K _{yy}	K _{yy} (m)	0.25 L _{pp}

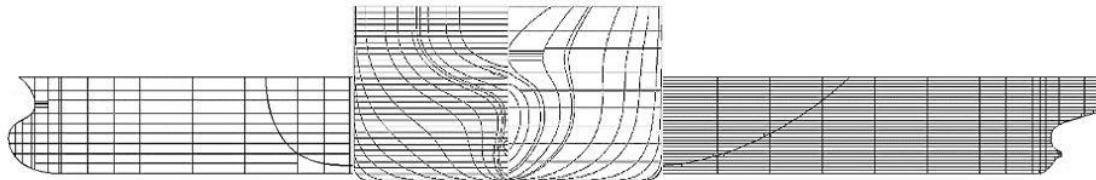


Fig. 2: Body plan and side view of the KVLCC2 ship model

The Japan Bulk Carrier (JBC) is a capesize bulk carrier jointly introduced by National Maritime Research Institute (NMRI), Yokohama National University and Ship Building Research Centre of Japan (SRC), for the Tokyo 2015 workshop. Table 3 provides specifications of the JBC model and Fig. 3 shows its side and body plan.

Table 3: Specifications of the bulk carrier ship model, JBC

Specification	Scale	JBC ship (full scale)
Length between perpendicular	L _{pp} (m)	280.0
Breadth	B (m)	45.0
Depth	D (m)	25.0
Draft	T (m)	16.5
Wetted surface area	S (m ²)	19556.1
Displacement volume	V (m ³)	178369.9
LCB from mid-ship (fwd+)	LCB (m)	7.133
K _{yy}	K _{yy} (m)	0.25 L _{pp}

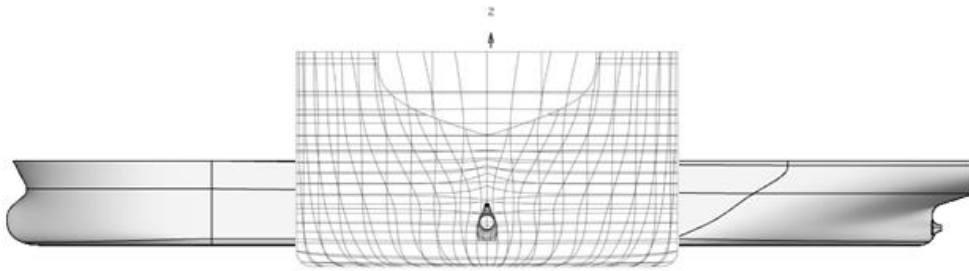


Fig. 3: Side view and body plan of JBC

2.3 Simulation Panels

For running simulation in HydroSTAR, 3D panel mesh was generated around the hull geometry using HydroSTAR mesh generation tool, HSMESH. HSMESH uses the body plan of ship and some information about the type of the fore and aft parts of the ship to generate the panel mesh. HydroSTAR reads the hull form using X, Y and Z coordinates. The hull form is to be divided in several sections in longitudinal direction and then each longitudinal section is divided into several vertical or radial sections. In the data set, each longitudinal section is represented by its X coordinate and the radial sections are by Y and Z coordinate. After HydroSTAR reads the hull form, HSMESH generates the panel mesh following defined number of panels.

The number of panels used for the JBC simulation was 300 by 50 for JBC, i.e., 300 section in longitudinal direction and 50 in radial direction. For KVLCC2, the number was 225 by 25, and that for KCS was 150 by 15. Fig. 4 shows the JBC hull surface (below water line) with panels. Although the figure also shows control surface for 2nd order drift load calculation, results of 2nd order drift load calculation is not shown in the paper.

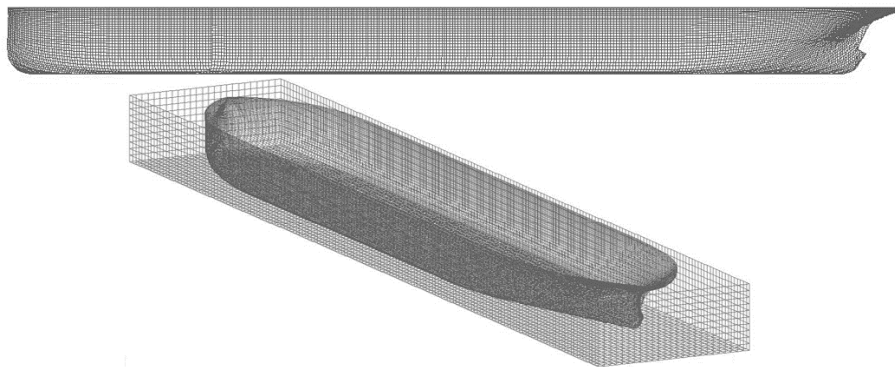


Fig. 4: Panel generated hull surface of JBC

As for panel size dependency in simulation, according to Pelaez et. al. (2000), for attaining panel size independent solution, the panel size in wave propagation direction should be less than 20% of the shortest wave length used in simulations. Furthermore, according to DNV, the diagonal of individual panel should be 1/6th of the shortest wavelength for proper convergence. The number of panel used for all three ship models are well within the stated limits. Thus, it may be considered that the attained simulation results are panel size or grid independent.

2.4 Computational resource

Generally, PF based codes are not high resource consuming and thus, PF based simulations can be performed in regular desktop computers. In this research, each simulation was performed in an Intel(R) Core i7 CPU with 8 cores, clock speed 2.27 GHz and 8 GB of physical memory. The solver took roughly 15 minutes to run each frequency step, with total time of simulation being roughly 7 hours.

3. Results and Discussions

Resistance and motion prediction results are shown in this section and analyzed to gain a comparative idea on ship resistance and related motion in different heading angles. However, the results are kept limited to short wave length cases, as the large commercial ship models simulated here are rarely exposed to wave lengths

beyond 0.8 of ship length in their regular voyage routes, Kim *et al.* (2013). The simulations were performed at design speed of the ships.

In head waves condition, the ship rides the wave with heave and pitch motion. Whereas, in case of the oblique waves, the waves are encountered mostly by one side of the hull. Thus, ship response changes. In this case, roll, sway and yaw motion become significant. In case of ships heading in head waves, the bulbous or blunt bow front encounters the incoming wave and motion is mostly limited to heave and pitch. However, in case of oblique waves, the wave is encountered mostly by one side of the hull and thus ship's motion response changes, and so does the resistance encountered. In this paper, head wave condition is represented by 180 deg. heading and following wave by 0 deg. heading, bow waves are represented by 150 deg. and 120 deg. angles, beam waves by 90 deg. and stern waves by 60 deg. and 90 deg.

3.1 Validation Study

HydroSTAR being a commercial code, has several validation studies available through numerous papers. However, being a PF based code, the solver's accuracy is limited to motion prediction, not resistance prediction. To validate the solver for the targeted simulations of this paper, both KCS and KVLCC2 model simulation results were compared with experimental data. However, experimental data could only be found for heave and pitch motion in head waves. Furthermore, wave simulation results are not available for JBC model, however, since JBC and KVLCC2 share similar hull form, validating KVLCC2 results should prove sufficient.

First, heave and pitch motion for the KVLCC2 model in head waves was validated using experimental data reported by Kim *et al.* (2013). The comparison is shown in Figure 5. The results show very good agreement with experimental data for heave motion. In case of pitch motion, results deviate with increasing wavelength. However, large ship like KVLCC2 rarely travel at wavelengths beyond 0.8L (Kim *et al.*, 2013). So present agreement level is sufficient for the presented study.

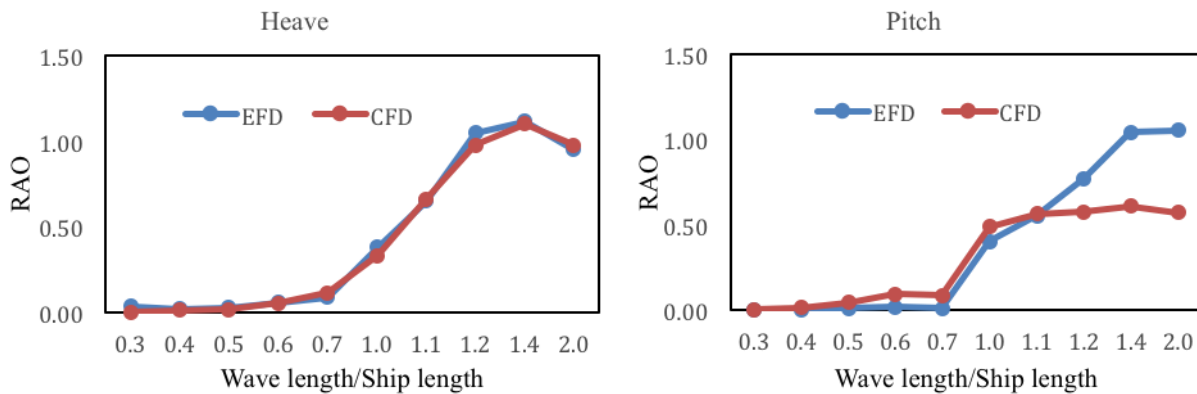


Fig. 5: Validation study for KVLCC2, heave and pitch motion

Next, validation study was performed for the KCS model using experimental data presented in Gothenburg 2010 workshop. The comparison for heave and pitch motion are shown in Figure 6. As can be seen from the Figure 6, both heave and pitch show significant deviation from the experimental data, however, the trend is well followed. Furthermore, the comparison is done only for a few data points since availability of experimental data is limited.

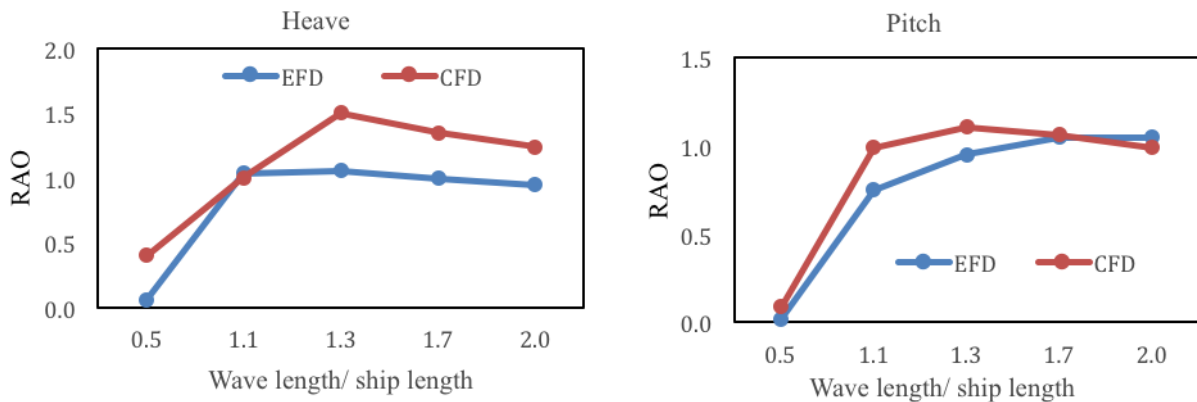


Fig. 6: Validation study for KCS, heave and pitch motion

Overall, the purpose of the present study is to understand the trend in ship resistance and motion in oblique waves, not to perform accurate measures of resistance and motion. Thus, for the intended study, present level of validation for both the ship models is sufficient.

3.2 KCS Model

The KCS is a container ship with a bulbous bow front. The bulbous bow increases wave making resistance, however, reduced frictional resistance and wave induced resistance. The resistance encountered by a KCS model at different wavelengths and in different heading conditions is shown in Figure 7. As can be seen from the Figure 7, ship encounters maximum resistance for encounter wavelength at head wave case. In bow wave cases, a gradual left shift is observed with a lower pick resistance value as heading shifts from head to beam wave heading. Resistance is minimum at beam wave and gradually increases from beam to following wave condition. The resistance encountered in oblique waves may be explained by the one-sided encounter of the wave by the hull. Such encounter although increases sway and yaw motion, reduces overall wave-induced resistance.

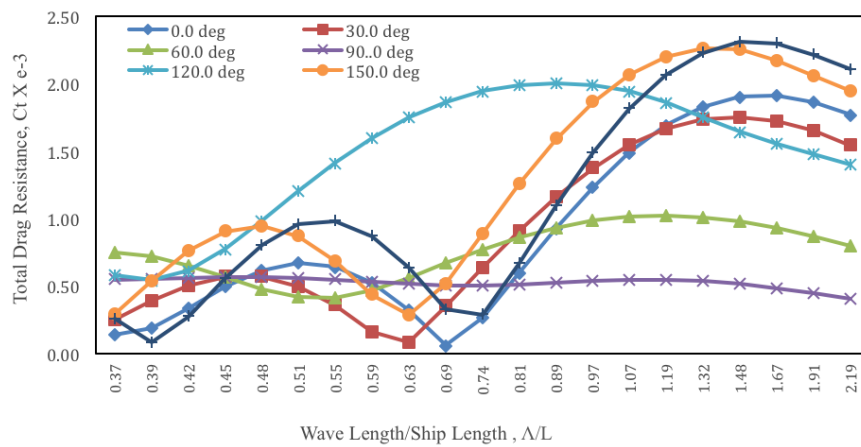


Fig. 7: Added resistance prediction for KCS in oblique waves

The heave RAO prediction shown in Figure 8 shows that a leftward shift is observed in heave motion from head to bow wave condition. Heave motion is significantly high at beam wave, irrespective of the encountered wave length. Heave motion gradually decreases from beam to following wave condition. Same observation can be made for pitch RAO shown in Figure 9, except pitch motion in beam wave is quite low comparing to heave motion and high pitch motion is observed at 60 deg. stern wave condition. As for surge motion (Figure 10), relatively high surge motion is observed at stern and following wave condition. Since, ship is propelled from stern section, wave from that region adds further thrust towards ship heading direction and results in higher surge motion.

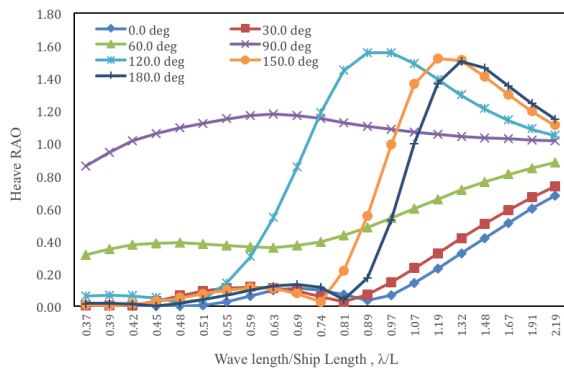


Fig. 8: Heave RAO prediction for KCS in oblique waves

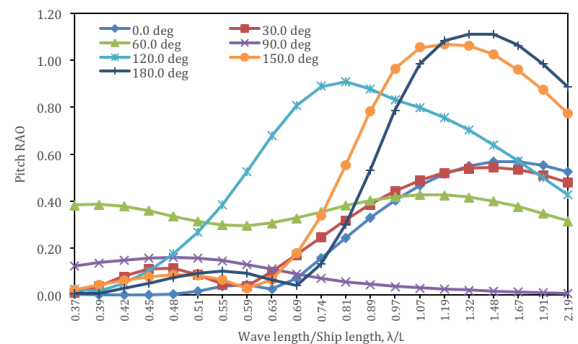


Fig. 9: Pitch RAO prediction for KCS in oblique waves

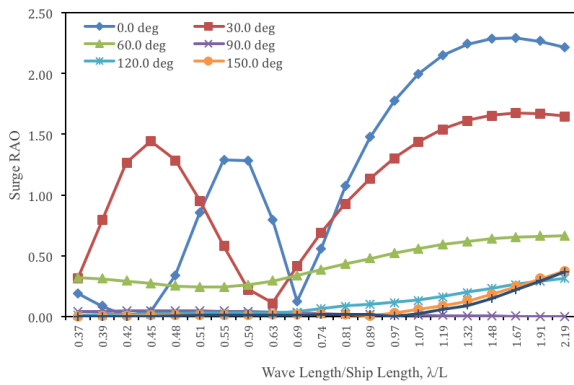


Fig. 10: Surge RAO prediction for KCS in oblique waves

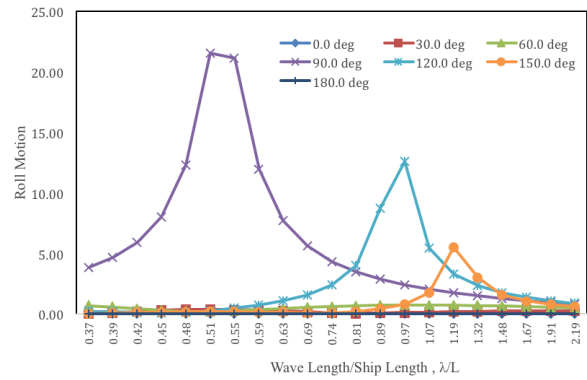


Fig. 11: Roll motion prediction for KCS in oblique waves

The roll motion prediction (Figure 11) shows that maximum roll motion is observed in beam wave condition, with maximum amplitude being at around 0.45L to 0.63L wave length, which may be close to the ship's roll resonance point. Resonance points can also be observed for 120 deg. and 150 deg. heading, which are at higher wave lengths with lower motion response.

As mentioned before, ship encounters higher sway and yaw motion at oblique waves, comparing to head waves, because of their one sided encounter of waves. As can be seen from Figure12, KCS encounters maximum sway motion at beam waves and almost negligible sway at head and following wave. In general, sway motion increases with higher wavelength, except for few headings, where sway response remains almost constant at higher wavelengths. As for yaw motion, the overall wave encounter area at stern section including the rudder is higher comparing the bow section. Thus, higher yaw motions are observed at stern waves comparing to bow waves, as can be seen in Figure 13.

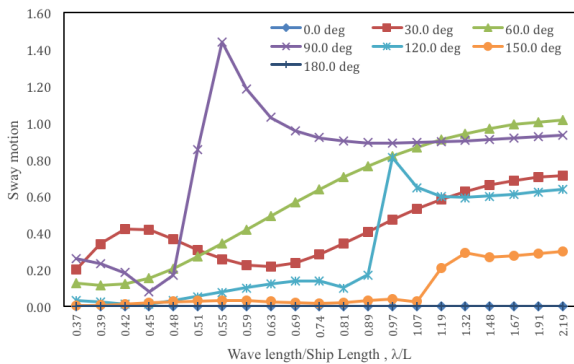


Fig. 12: Sway motion prediction for KCS in oblique waves

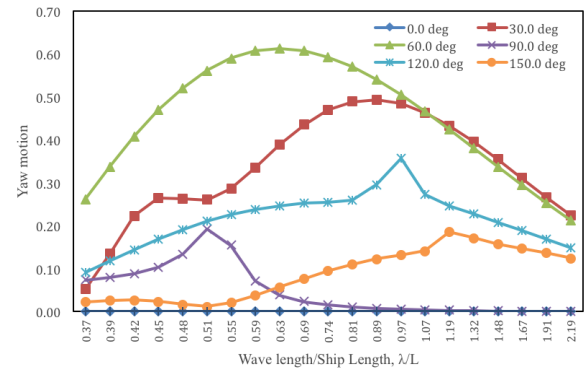


Fig. 13: Yaw motion prediction for KCS in oblique waves

3.3 KVLCC2 Model

The KVLCC2 is a crude carrier with a blunt bow front. The blunt bow gives the ship a wave riding motion and reduces wave-induced resistance. The resistance encountered by a KVLCC2 in head and oblique waves at different wavelengths has been shown in Figure 14. Although the predicted results show high deviation with experimental data, it does provide comparative data for ship resistance at different heading angles. As can be seen from the figure, ship encounters maximum resistance at head wave condition, if encounter waves are considered. With heading changing from head to bow wave conditions, resistance curve takes a leftward shift with reduced peak resistance amplitude. At beam wave resistance is minimum and is negligibly affected by the incoming wavelengths. Resistance increases again from beam to following wave, with maximum resistance being at 60 deg. heading.

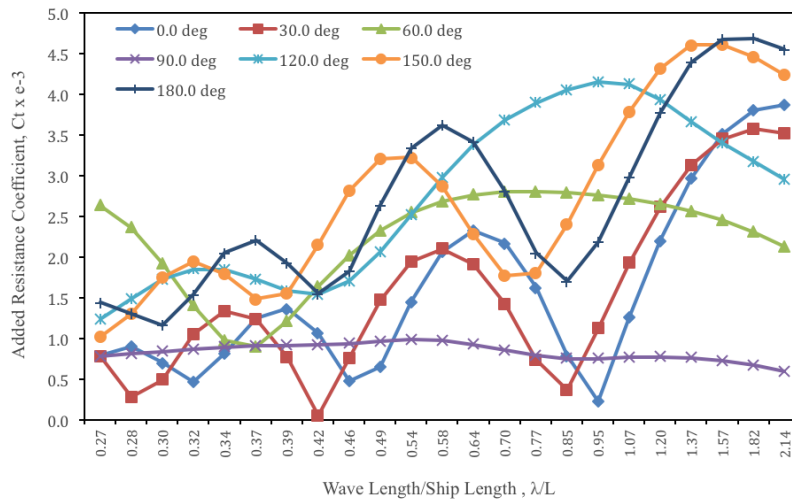


Fig. 14: Added resistance prediction for KVLCC2 in oblique waves

Maximum heaving motion is observed at beam wave for a KVLCC2, as can be seen in Figure 15. Minimum heaving motion is observed at head and following waves, which continuously increases with increasing heading angle. A relatively high heave motion is observed for 60 deg. heading, irrespective of the encountered wavelength. The pitch motion prediction shown in Figure 16 reveals that maximum pitch motion is observed during head wave motion, which may be explained by the blunt bow front of the ship, which gives wave riding motion. Bow heading conditions show a continuous lift shift in motion curve with decreasing heading angle. Pitch motion is minimum at beam wave and is quite high at 60 deg. heading, which may be explained by the smaller wave encounter area at stern section.

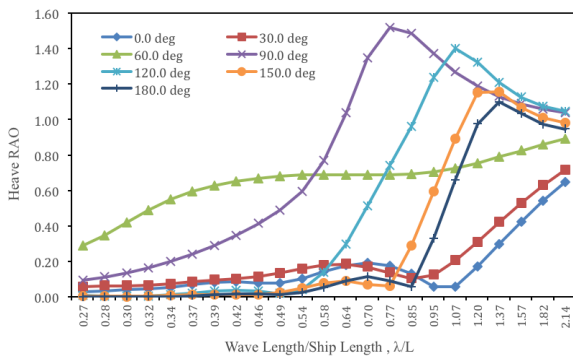


Fig. 15: Heave RAO prediction for KVLCC2 in oblique waves

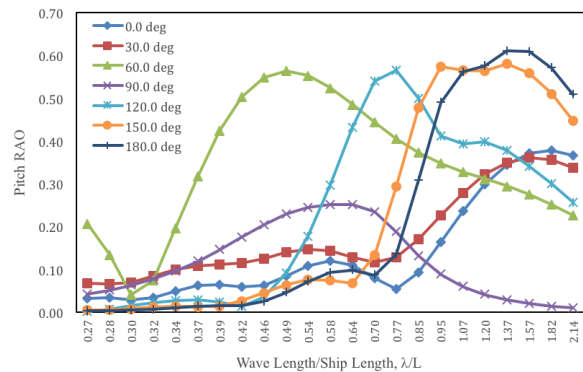


Fig. 16: Pitch RAO prediction for KVLCC2 in oblique waves

According to Figure 17, relatively higher surge motion is observed at following and stern waves, comparing to head, bow and beam waves. Overall difference in surge motion for head and bow wave is minimum. The roll motion prediction shown in Figure 18 shows that roll motion is maximum at beam waves and the peak value is at 0.77L wavelength. Roll motion is comparatively higher for heading angles close to beam waves, which may be explained by the wave encounter area of the ship. For head, bow, stern and following waves, roll motion remains minimum.

Ship encounters almost zero sway motion at head and following waves, which gradually increases towards beam wave condition, as shown in Figure 19. In Figure 20, maximum yaw motion is observed at stern waves with 60 deg. heading, which may be explained by the relatively large wave encounter area including rudder. Yaw motion is minimum at head; following and beam wave, and is comparatively higher at stern waves comparing bow waves.

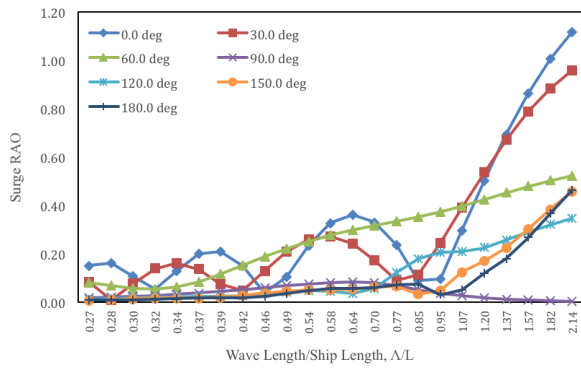


Fig. 17: Surge RAO prediction for KVLCC2 in oblique waves

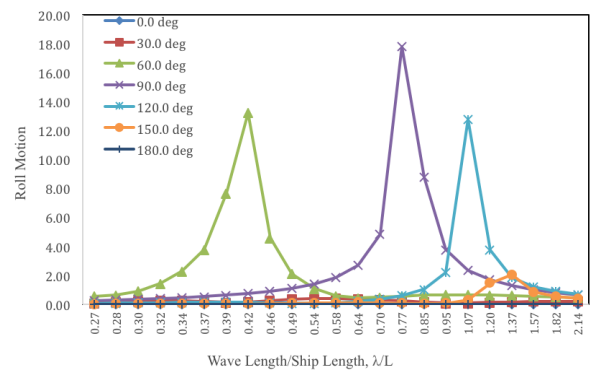


Fig. 18: Roll motion prediction for KVLCC2 in oblique waves

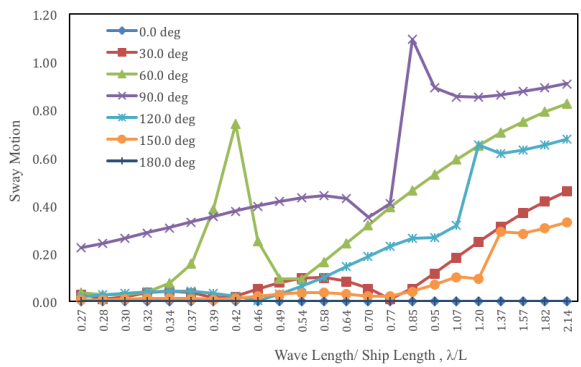


Fig. 19: Sway motion prediction for KVLCC2 in oblique waves

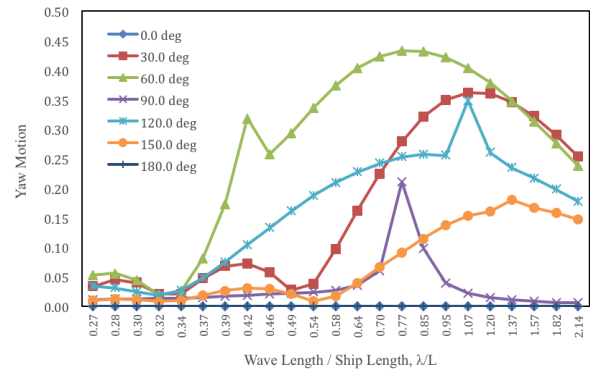


Fig. 20: Yaw motion prediction for KVLCC2 in oblique waves

3.4 Japan Bulk Carrier (JBC) model

The Japan Bulk Carrier (JBC) is a bulk carrier model with a blunt bow. The resistance prediction for the ship has been shown in Figure 21. It can be seen from the figure that the resistance encountered by the ship is maximum in head wave and is minimum in beam wave motion. In general, the resistance curve shows a leftward shift from head to following wave condition; the resistance amplitude is also reduced.

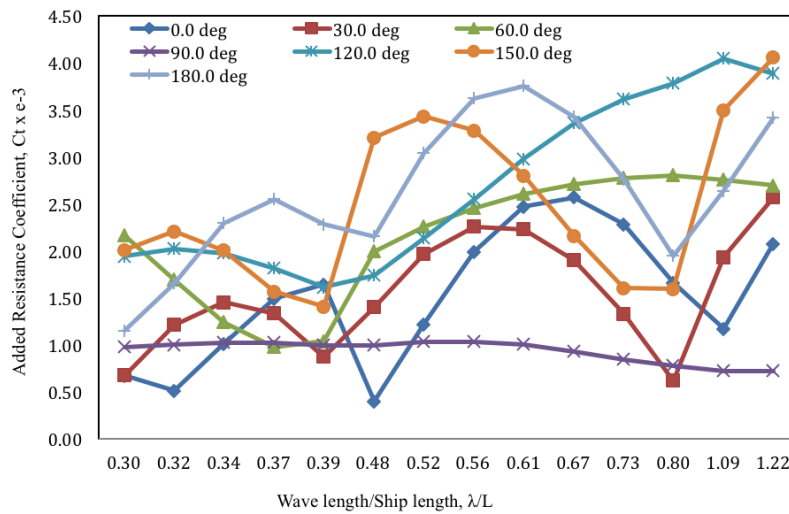


Fig. 21: Added resistance prediction for JBC in oblique waves

From motion prediction results, the heave RAO results show that maximum heave motion (Figure 22) is gained at beam wave condition and minimum at head waves. In short wavelength cases, heave motion varies slightly against heading angle, however, at higher wavelengths, the variation is significant. Pitch motion prediction in Figure 23 shows that maximum pitching motion is observed in 60 degree and 120 degree heading. Similar to heave motion, pitch motions show little variation for different heading angles for short wave cases. In case of surge motion (Figure 24), higher motion is observed in case of stern and following wave cases, comparing to head and bow wave cases.

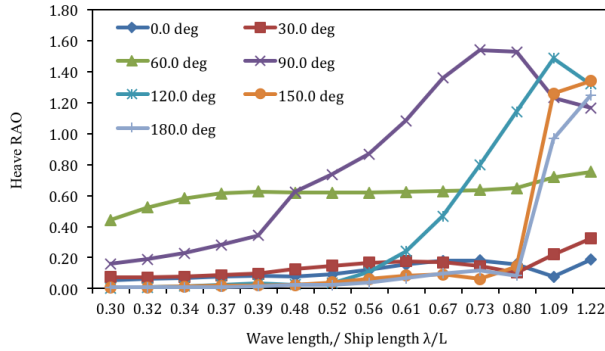


Fig. 22: Heave RAO prediction for JBC in oblique waves

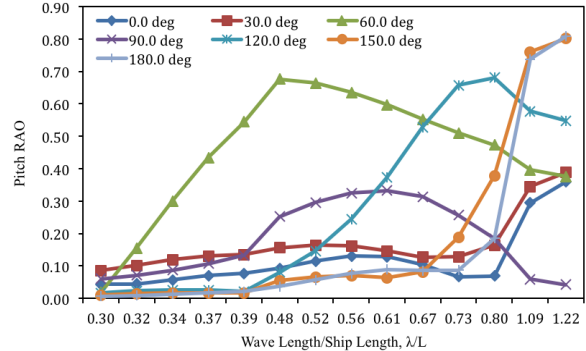


Fig. 23: Pitch RAO prediction for JBC in oblique waves

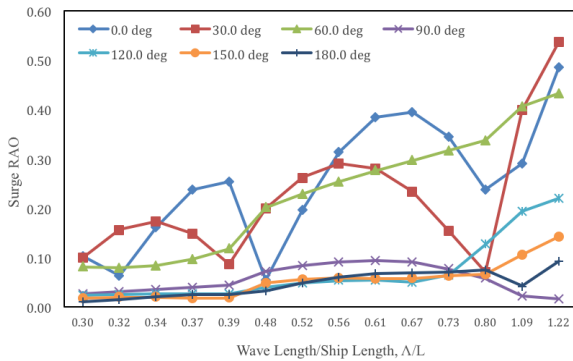


Fig. 24: Surge RAO prediction for JBC in oblique waves

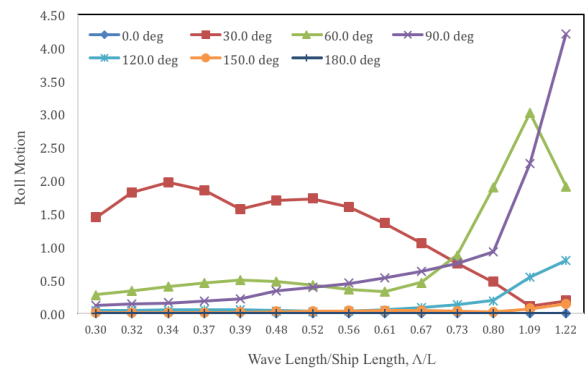


Fig. 25: Roll motion prediction for JBC in oblique waves

Fig. 25 shows that high roll motion is observed for stern waves, whereas, roll motion remains minimum for head and following wave cases. However, maximum roll motion is expected in beam wave condition, whereas, the result shows that maximum was observed in 60 degree heading, which might be a numerical flaw. Maximum sway motion is observed in beam wave condition, as shown in Figure 26, which is natural considering continuous side impact on hull by waves. As for yaw motion (Figure 27), maximum yaw displacement is observed at 60 degree heading.

4. Conclusion

The paper presented resistance and motion prediction for a container carrier, a tanker ship and a bulk carrier using a potential flow based solver, in different oblique waves and how motion and resistance of ship changes with heading angle with respect to incoming wave direction. In general, ships show maximum resistance at head wave cases considering the encounter wavelength and minimum at beam wave condition. However, at beam wave ships encounter high heave, roll and sway motion. Stern wave conditions encounter less resistance comparing to bow wave conditions, however, pitch motion encountered at stern waves are lower. The influence of heading angles in ship's resistance and motion has been revealed in this paper with an intention that it can serve as a reference for shippers and mariners for selecting voyage routes and heading angles depending on their priorities. This paper also established the applicability of HydroSTAR for prediction of resistance, motion of ship in various wave headings.

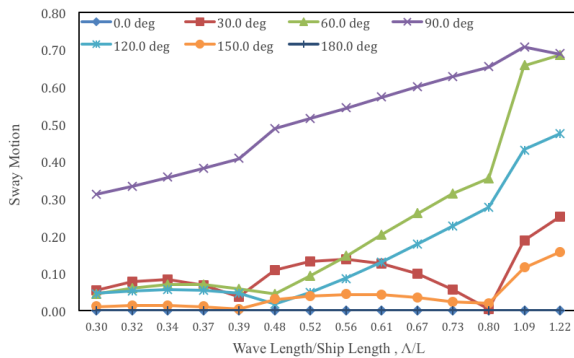


Fig. 26: Sway motion prediction for JBC in oblique waves

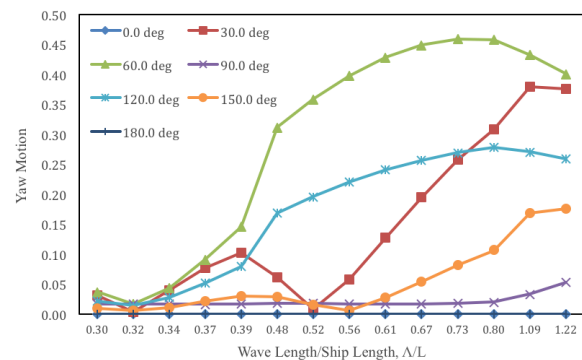


Fig. 27: Yaw motion prediction for JBC in oblique waves

Acknowledgement

In present research, HydroSTAR software is used with the permission obtained through an MOU between Bureau Veritus and Bangladesh University of Engineering and Technology.

References

- Chan, H. S., Atlar, M. and Incecik, A. (2002): Large-amplitude motion responses of a Ro-Ro ship to regular oblique waves in intact and damaged conditions, *Journal of Marine Science and Technology*, vol. 7, pp. 91-99. <https://doi.org/10.1007/s007730200017>
- Chen, J. P. and Zhu, D. X. (2010): Numerical simulations of wave-induced ship motions in regular oblique waves by a time domain panel method, *Journal of Hydrodynamics*, Vol. 22 (5), pp. 419-426. [https://doi.org/10.1016/S1001-6058\(09\)60230-4](https://doi.org/10.1016/S1001-6058(09)60230-4)
- Chen, X. B. (2004): Hydrodynamics in offshore and naval applications-Part I, 6th International Conference on Hydrodynamics, Perth, Australia.
- Chen, X. B. and Rezende, F. (2009): Efficient computations of second-order low-frequency wave loads, 28th International Conference on Offshore Mechanics and Arctic Engineering, Honolulu.
- Chuang, Z. and Steen, S. (2013): Speed loss of a vessel sailing in oblique waves, *Ocean Engineering*, vol. 64 (2013). <https://doi.org/10.1016/j.oceaneng.2013.02.018>
- Chuang, Z. (2013): Experimental and numerical investigation of speed loss due to seakeeping and maneuvering, Doctoral Thesis, NTNU.
- Duan, W. and Li, C. (2013): Estimation of added resistance for large blunt ship in waves, *Journal of Marine Science and Application*, vol. 12, pp. 1-12. <https://doi.org/10.1007/s11804-013-1177-6>
- Kim, J., Park, I.R., Kim, K.S., Kim, Y. C., Kim, Y. S. and Van, S. H. (2013): Numerical towing tank application to the prediction of added resistance performance of kvlcc2 in regular waves, *Proceedings of the Twenty-third (2013) International Offshore and Polar Engineering (ISOPE) Anchorage, Alaska, USA*.
- Kumar, A. (2014): Numerical computation of hydrodynamic forces and motions of TLP using 3D source distribution technique, M.Sc. Engg. Thesis, Dept. of NAME, BUET.
- Ming, W., Guo, S. A., Bo, Y., Xiao, W. and Chao, W. Z. (2013): Simulation research on three DOF motions of ship in oblique waves based on CFD, *Application Research of Computers*, vol. 30 (7).
- Pelaez, J. G., Papanikolaou, A. and Gonzalez, V. (2000): Numerical and experimental study on the seakeeping performance of a fast round-bilge mono hull. *Proceedings of the 4th Osaka Colloquium on Seakeeping Performance of Ships*, Cosmosquare Int. Education and Training Center, Osaka, Japan.
- S. (2008): SIMMAN 2008. [Online], Available: <http://www.simman2008.dk/>. [Accessed 2016].
- Song, N. J., Kim, K. H. and Kim, Y. (2011): Numerical analysis and validation of weakly nonlinear ship motions and structural loads on a modern containership, *Ocean Engineering*, vol. 38, pp. 77-87. <https://doi.org/10.1016/j.oceaneng.2010.09.017>
- T. (2015): Tokyo 2015 Workshop, [Online]. Available: <http://www.t2015.nmri.go.jp/jbc.html>. [Accessed 2016].
- Orihara H. (2005): Development and application of CFD simulation technology for the performance estimation of ship in waves, Ph.D Thesis (in Japanese), The University of Tokyo, Japan.